Force-Distance Relation for Dental Magnets - Fitted Equation

ABSTRACT

Objective: The force-distance power law for dental magnets had been unresolved until a theoretical study found that only even inverse powers were allowed; for simple magnets inverse fourth power was the only possibility. It remained to demonstrate that this indeed did apply to real magnets, the present purpose. Methods: The force exerted by a series of real dental magnets to a large steel plate, and in a few cases to dental magnet keepers, as a function of distance was recorded. Curve-fitting of that data was explored. using the equation previously used for long dipoles, but allowing the power to be a free parameter. An index of 4 was the only feasible value. Corresponding fitted parameter values were then examined in relation to magnet design and each other. Results: The theoretical power law index was confirmed to be 4. For a satisfactory fit, a 'polar offset' and a 'stretch power' were again required to better approximate the experimental results. Polar offset appears to be a function of apparent pole strength; stretch power less clearly so. Significance: The motivating question is settled.

Keywords

Power Law
Dental Magnets
Force-Distance Equation
Breakaway Force

Authors

Brian W. Darvell *
(DSc, FRSC, FIMMM, FADM)

Andrew P. Dias §
(BDS (Cey), MDS (S'pore), FDSRCPS (Glasgow), MPhi (HK))

Address for Correspondence

Brian W. Darvell *

Email: b.w.darvell@bham.ac.uk

* *School of Dentistry, The University of Birmingham, Birmingham, UK*

§ *Royal Dental Hospital Melbourne, 720 Swanston Street, Carlton. VIC, Australia.*

Received: 11.05.2022
Accepted: 29.07.2022

doi: 10.1922/EJPRD_2440Darvell19

INTRODUCTION

As has been previously discussed,[1,2] miniature magnets are used in dentistry for denture retention and orthodontic treatment, and understanding the relationship between the force exerted on a keeper and its separation from a magnet would be of value for design and application. However, for various reasons, there has been no consensus as to the nature of that relationship, with imprecise and contradictory experimental determinations.

From the earliest work,[3] the inverse square law has been said to apply, although this can only be true for the interaction between a single pair of point-like poles. Elliot (1988)[4] cited Gillings (in a personal communication) as remarking that the field strength drops as the inverse cube of distance, although no publication regarding this has been traced and thus no grounds are known for the assertion.

To begin to address the problem of the force-distance relationship for dental magnets, and as a simplification, the behaviour of long, thin cylindrical magnets against a magnetizable stainless steel disc was studied as an approximation of a 'pole' and its image in a permeable plane (that is, with the other end of the unavoidable dipole sufficiently distant as to be non-contributory),[1] when it was found that the inverse-square (Coloumb) law did not apply as such. This was attributed to the fact that a polar disc – rather than a point – might be a better approximation, but even the rigorous mathematical solution to this model failed to match behaviour.[2]

Instead, by inspection and exploration, a simple function was found:

$$F = \frac{a}{(d^c + h)^2} \quad (1)$$

that, allowing for minor zeroing errors in force, *F*, and separation, *d*, gave a satisfactory fit. Here, *a* is a general scale factor representing the effect of the magnet strength and *h* was taken to be a polar-disc offset (that is, of its location inside the face of the magnet), while *c* is a curvature adjustment (equivalent in effect to the 'stretched exponential' previously applied).[1] This was shown to be the most parsimonious expression feasible.

The question remains as to the behaviour of real dental magnets, as opposed to the simplified system studied before.[1,2] Here, it is not just a case of the summation of effects for a simple point dipole and its image, but it is apparent that the 'polar patch' equivalent must be used in any mathematical treatment. The situation becomes even more difficult when more complicated magnet designs are involved. The mathematical problem was solved for any arbitrary arrangement of magnetic poles,[5] using as a basis the established physical Coulomb law for the interaction of pairs of point-like poles, and thus for the integration of the effects over surfaces and volumes: only inverse power laws with even integer powers are permissible at large separations. Nevertheless, it was found that the real, physical data for the long thin dipoles,[1,2] did not fit that solution at small *d*, even though the asymptotic behaviour at large *d* was as expected – inverse square. For a dipole and its image, inverse fourth power is expected at large *d*, with which previous results[6,7] appear, at least, to be consistent. Thus, given the success of the curve-fitting for the long, thin dipole magnets,[2] the behaviour of dental magnets was re-examined.

MATERIALS AND METHODS

Sixteen brands of dental magnet, from eight manufacturers, were tested (*Table 1*). The same equipment and approach as before was used,[1] with all due care being taken to ensure a stable result after each cross-head movement, generally requiring a few minutes to settle, also correcting displacement for load-cell compliance. The sequence of tests was more or less random, collected over a long period of time, such that long term systematic effects are unlikely.

Because the theoretical mathematics of the force-distance relationship is extremely complicated[5] it is not possible to use those results to analyse the experimental results. Hence, in the manner previously used,[2] a wide array of equation forms was explored through curve-fitting in software (TableCurve 2D v5.0, SPSS, Chicago, IL, USA), checking both by visual inspection of plots and the physical sense of the fitted parameter estimates. The most parsimonious, general, and effective function, following the structure of equation (1) in [2], was:

$$F = \frac{a}{\left[(d + \varepsilon_d)^c + h\right]^4} + \varepsilon_F \quad (2)$$

where now the fitted 'zeroing' error terms for force and displacement are shown (as used previously).

Given the large range of force values involved – a few newtons down to millinewtons, better stability was obtained using fitting log(*F*) to the log of the right-hand side, because of which it was found convenient to treat the breakaway force (i.e. the peak value) as occurring at 0.1 μm, to avoid singularities in the various function explorations. In addition, better stability and ease of graphical inspection was obtained by scaling the separation *d* and using the log value as input. Thus the data transforms were:

$$X \rightarrow \log(X/1000),\ Y \rightarrow \log(Y) \quad (3)$$

and the fitted function:

$$Y = \mathrm{LOG}(\#A/(\#B + ((10\text{^}(X) + \#E)\text{^}\#D)\text{^}4 + \#C) \quad (4)$$

where #A = a; #B = 'polar' offset, *h*; #C = zeroing error in *F*, ε_F; #D = stretch power, *c*; #E = zeroing error in *d*, ε_d. The order of the constants is as they were found necessary to be included for a satisfactory fit across the data set.

The denominator exponent was initially allowed to be a free parameter for the fitting. It was found that in several instances the model was thereby effectively overspecified and unusable results obtained. Otherwise, the value tended to lie in the region of 4, which conformed with the prediction.[5] To be sure, fixed values of 2 and 6 were also checked but failed to provide even a suggestion of a satisfactory fit.

The procedure was necessarily somewhat recursive. By inspection, obviously errant values of force (being clearly outside the noise envelope), possibly attributable to transcription error or system glitch, were deleted. Fewer than 1% were thus affected. More problematic was that at values less 10 mN system drift became obvious, bearing in mind that a run could take several hours, despite air-conditioning and allowing the test machine to stabilize overnight (> 16 h). This necessitated the trimming of that late data when there was a sequence of three of more points deviating appreciably from the trend of the previous.

RESULTS

The cleaned raw data are shown in Figure 1, where two examples of that kind of deviation requiring trimming are also shown. Subsequently, inspection of the fitted curve might show an occasional obviously errant point or deviating trend; these were removed and the fit recalculated. Generally, the standard errors would be improved without the parameter estimates being affected materially.

In the majority of instances, the value of the estimate of the zeroing error in distance was found to be insignificantly different from zero and this led to an overfitted function with

Table 1. Characteristics of magnets tested, showing design icon used in Figures 4 - 7 and Supplementary Figures 1 and 2, and the symbol colour for all plots.

Manufacturer	Product name	Height / mm	Diameter / mm	Alloy	Field type	Assembly design	Cladding or Case	Pole-piece	Group
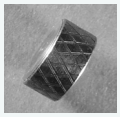 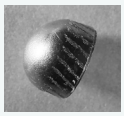 Golden Dental Products, Savannah GA, USA	GDP Maxi	3.0	4.58	NdFeB	Open	nil (dipole)	Ti	ND	1a
	GDP Mini	2.35	4.58	NdFeB	Open	nil (dipole)	Ti	ND	1b
	GDP Igloo	2.95	4.4	NdFeB	Closed	Sandwich	Ti	ND	1c
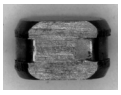 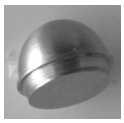 Innovadent, Pymble NSW, Australia	Maxi	3.6	6.2 × 4.0	CoSm	Closed	Split-pole	SS	SS	2a
	Neomini	3.35	4.5	NdFeB	Closed	Sandwich	SS + "surface coating"	SS	2b
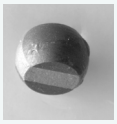 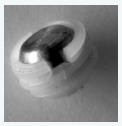 Preat, Grover Beach, CA, USA	Shiner Regular	3.1	4.7	NdFeB	Closed	Sandwich	SS	ND	3a
	Shiner Small	2.6	3.8	NdFeB	Closed	Sandwich	SS	ND	3b
 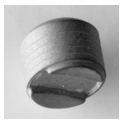 Solid State Innovations, Mt. Airy, NC, USA	Jackson Regular	3.8	5.5	NdFeB	Closed	Sandwich	SS	Ni-Cr plated	4a
	Jackson Small	3.1	4.5	NdFeB	Closed	Sandwich	SS	Ni-Cr plated	4b
 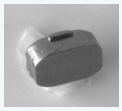 Aichi Steel, Tokai-shi, Japan	Magfit Magnedisc 800	1.4	4.4	NdFeB	Closed	Circular	SUS 316 (SS)	AUM20 (SS)	5a
	Magfit EX 600	1.8	2.8 × 3.8	NdFeB	Closed	Sandwich	SUS 316 (SS)	none	5b
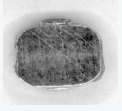	Magfit EX 400	1.5	2.4 × 3.4	NdFeB	Closed	Sandwich	SUS 316 (SS)	none	5c
 Technovent, Leeds, UK	Magna-cap mini	3.1	5.4	NdFeB	Closed	Split-pole	SS	ND	6

Table 1 continued overleaf

Table 1 continued. .

Manufacturer	Product name	Height / mm	Diameter / mm	Alloy	Field type	Assembly design	Cladding or Case	Pole-piece	Group
 Magne-Dent Zest Anchor, San Diego, CA, USA 	MagneDent Large	2.8	5.1	NdFeB	Closed	 Circular	SS	ND	7a
	MagneDent Small	2.5	4.0	NdFeB	Closed	 Circular	SS	ND	7b
 Dyna Dental Engineering, Bergen op Zoom, Netherlands 	Dyna	2.4	4.8	ND	Open	 (nil) dipole	**	ND	8

SS: Stainless steel ND: Not described **"biocompatible non-corrosive alloy"

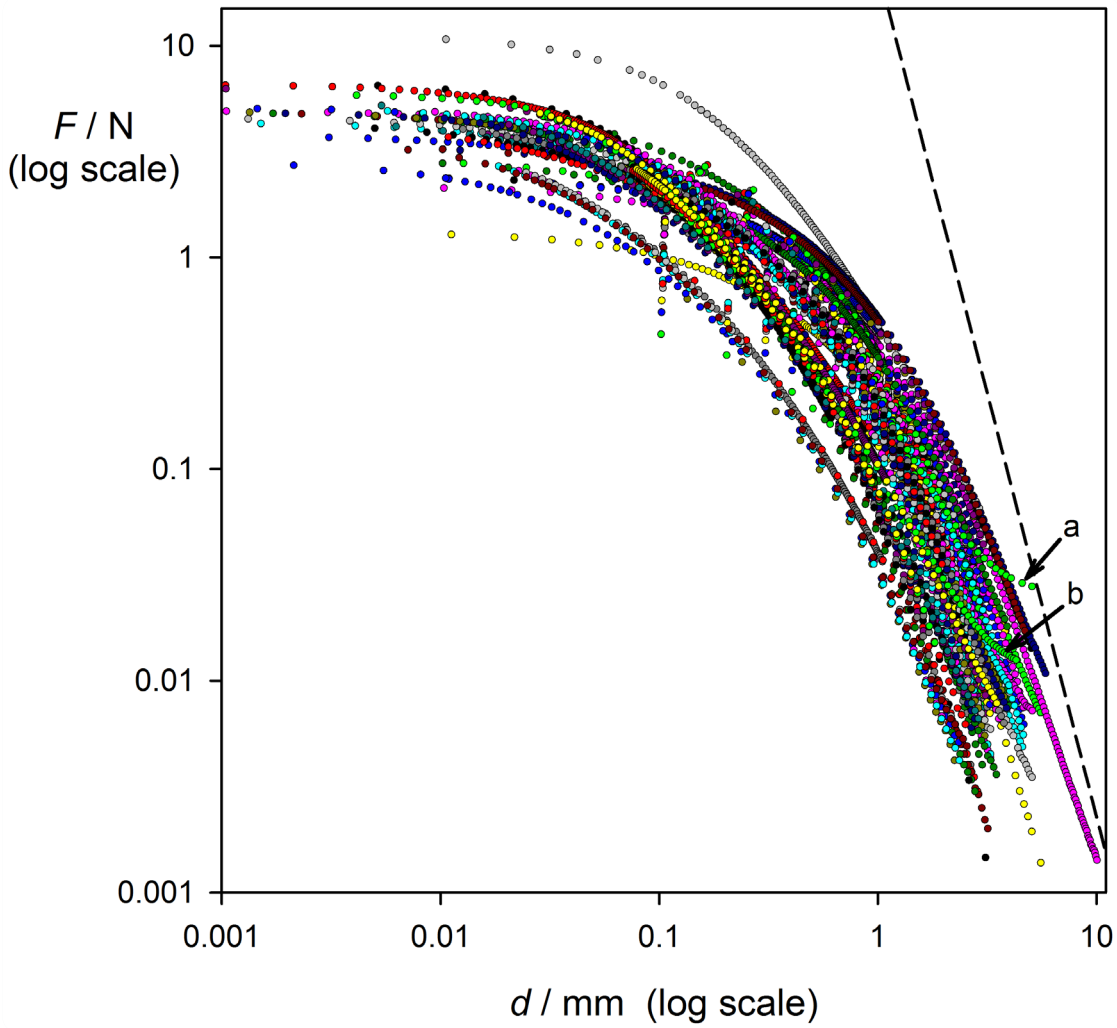

Figure 1: Raw data for all magnets after trimming deviating points at very small and very large separations (see text). Two examples of drift at large separation have been left to indicate the nature of the problem: from a) Group 6, b) Group 3a. The dashed line is of slope -4. (Breakaway values not shown.)

consequent larger standard errors in the other parameter estimates (which were then insignificant). Dropping that parameter then gave a much better fit with no insignificant values. In 20 instances, this was also true of the estimated zeroing error in force, after the distance error had been dropped because that was the most destabilizing, when a similar procedure was followed.

The curve fitting results are shown in Figure 2, where the raw data have been transformed as indicated:

$F \rightarrow F - \varepsilon_F$ and $d \rightarrow (d + \varepsilon_d)^c + h$.

The linearization is notable with the exception of a few deviations at low *d*. Rescaling the ordinate by dividing by *a* (*Figure 3*) shows that the outcome is consistent and that the inverse fourth power is the applicable limiting form for all magnets.

The principal measure fitted was the 'strength', *a* (equation 1), and this was rescaled to yield the apparent pole strength Q from the relevant relationships using:

$$Q = \sqrt{\frac{a}{10^{-7}}\left(\frac{\mu_r - 1}{\mu_r + 1}\right)} \qquad (5)$$

taking the permeability of free space as $4\pi \times 10^{-7}$ Hm^{-1}, and the relative permeability of stainless steel (the opposing permeable plane) as 200.[1] The results are shown in Figure 4 by product. The fitted values for 'offset', *h*, are likewise plotted in Figure 5, and the 'stretch' power in Figure 6.

For comparison and exploration, plots of the breakaway force, F_{max} by product (*Figure 7*), as well as pairwise plots of each fitted parameter (*Figures 8 - 13*) and a 3D view of power vs. pole strength and offset (*Figure 14*) are also given. The full fitted data set is given in Supplementary Table 1.

DISCUSSION

There were several challenges in obtaining the raw data. Given that both force and separation ranged over four orders of magnitude, and the long duration required for any run, thermal and electronic drift frequently became problematic at large separations, despite all precautions. Also, the machine resolution of just 1 μm (the limit of the encoder) would appear to be inadequate for the present purpose at small separations; an optical (non-contact) displacement sensor (e.g. as used here[8]) might be of value if capable of higher resolution. Thus, both ends of the range have experimental difficulties. In addition, it became apparent that breakaway force reproducibility was sometimes poor, despite ensuring cleanliness for good contact and frequent degaussing of the stainless steel. This then showed in the scatter in estimated parameter values for replicate runs (see identified replicates in Supplementary Table 1). It is apparent that further measures would need to be taken to improve on the data quality, underlining the comments made earlier,[1,2] if this kind of work is to be contemplated. Nevertheless, it is clear that

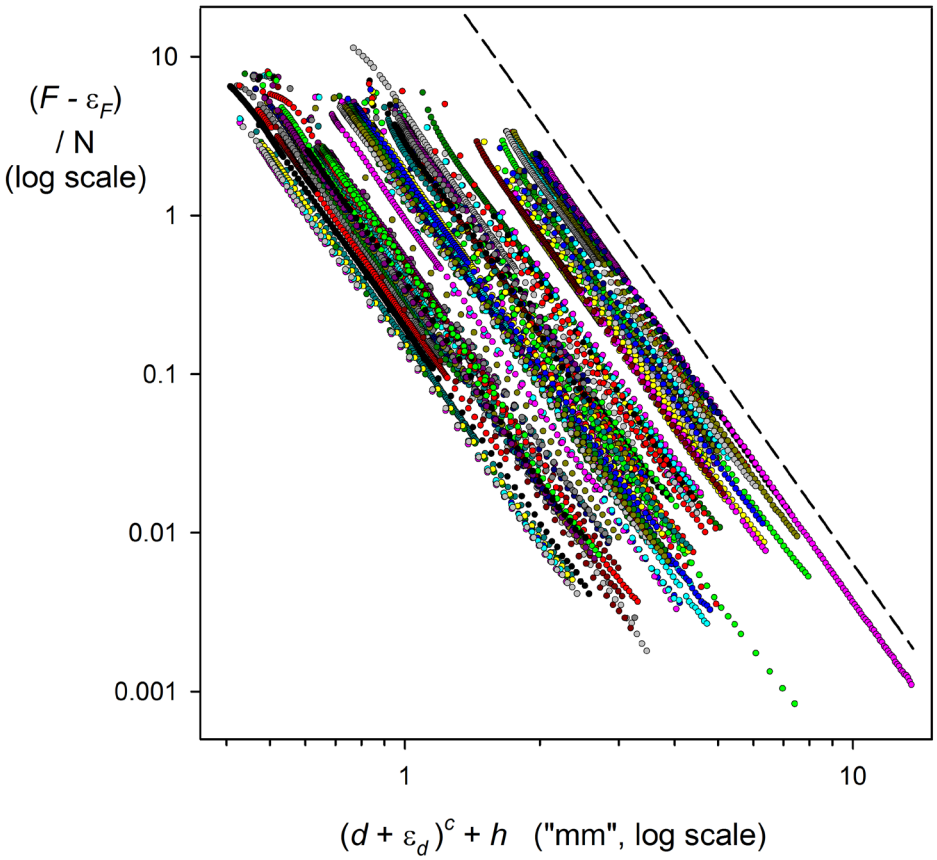

Figure 2: Data of Figure 1 rescaled according to the fitted parameters. (The untrimmed examples are now trimmed.)

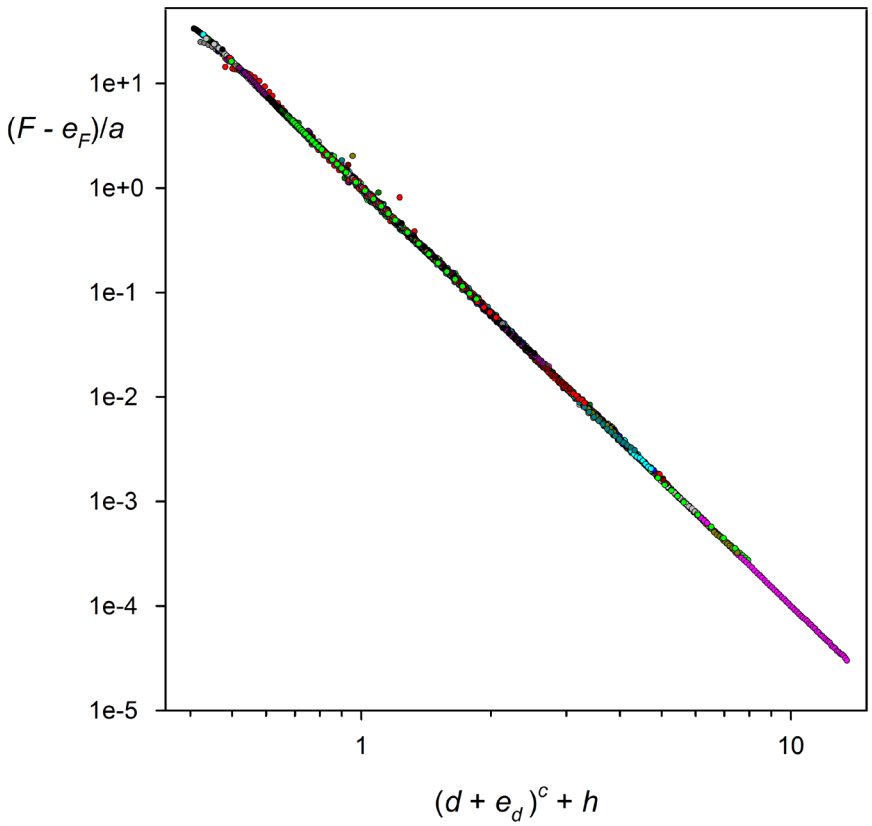

Figure 3: Data of Figure 2 rescaled by the force scale factor *a*. There is a good approach to the expected straight line over 5 orders of magnitude.

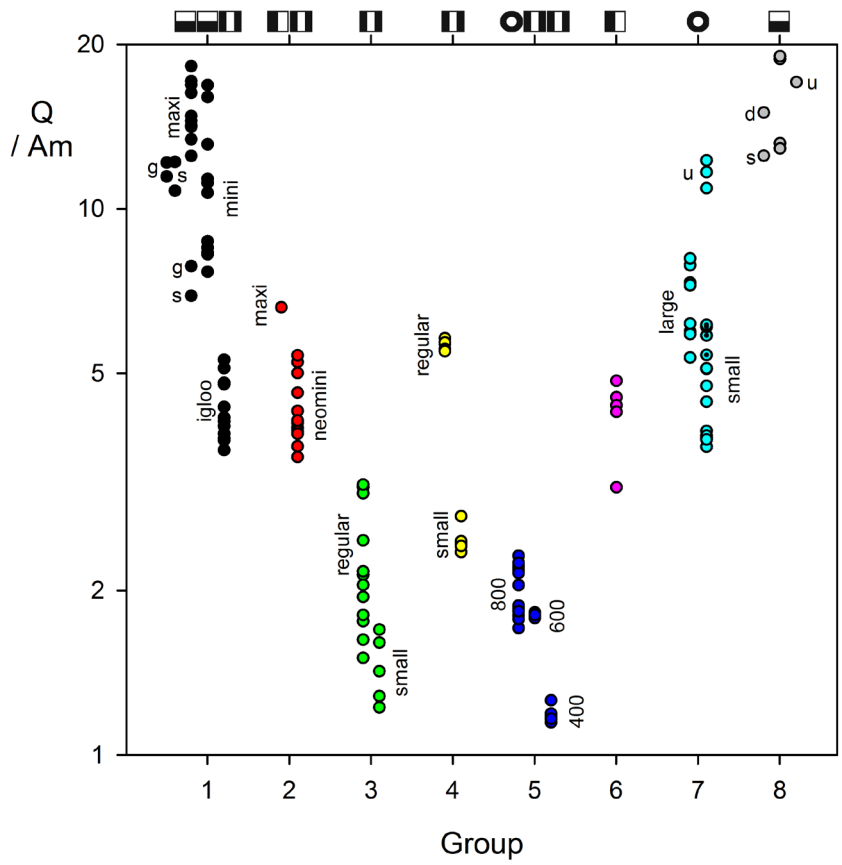

Figure 4: Calculated apparent 'pole strength', Q, by magnet type from fitted values of *a*. The icon on the upper border represents the magnet design (see Table 1). Key labels have been inserted where useful to distinguish products. Points where commercial keepers were tested indicated by letters: d - Dyna, g - GDP, s - Shiner. Unclad magnets : u.

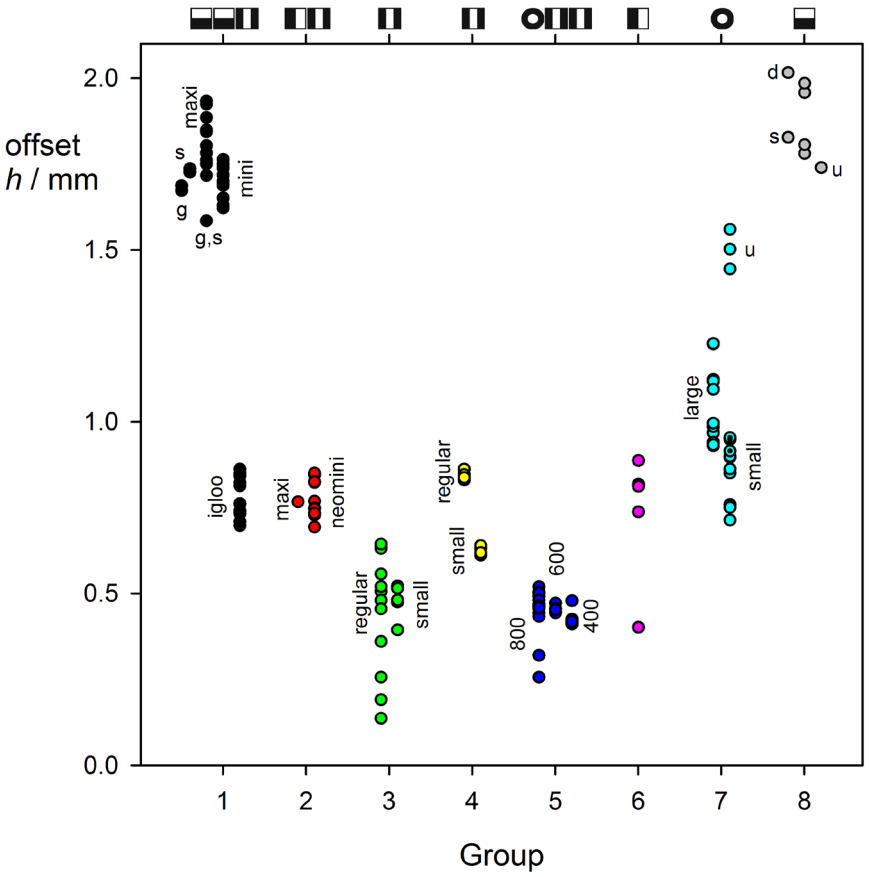

Figure 5: Fitted values of the apparent polar offset, *h*, by magnet type. Key as for Figure 4.

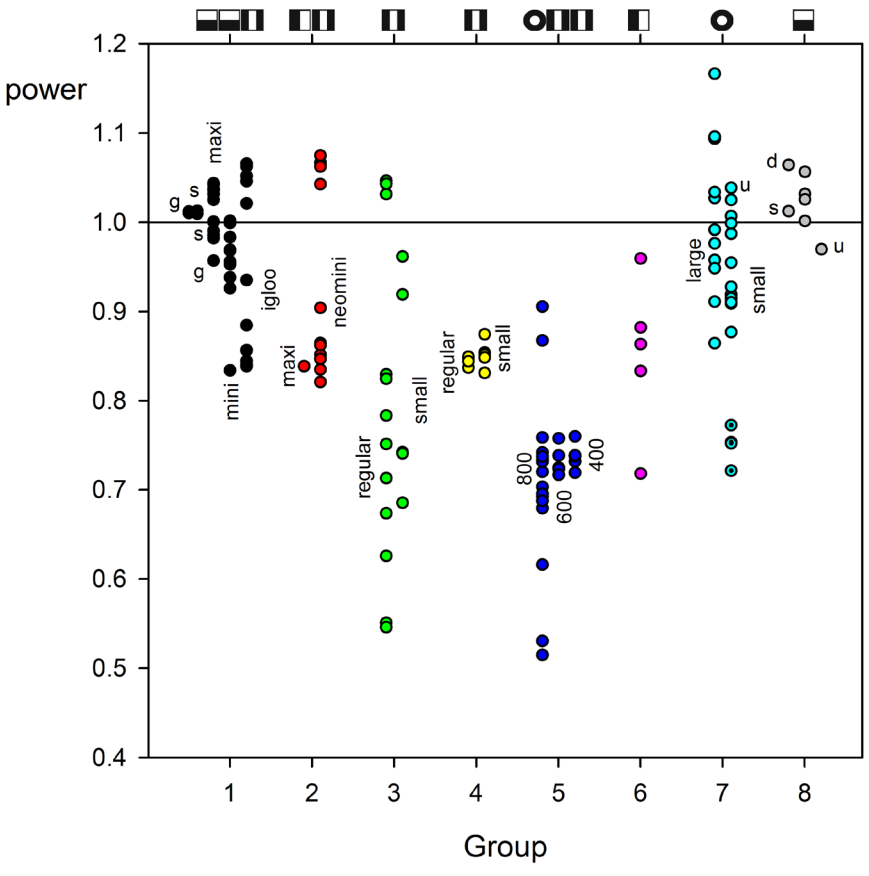

Figure 6: Fitted values of the apparent stretch power, *c*, by magnet type. Key as for Figure 4.

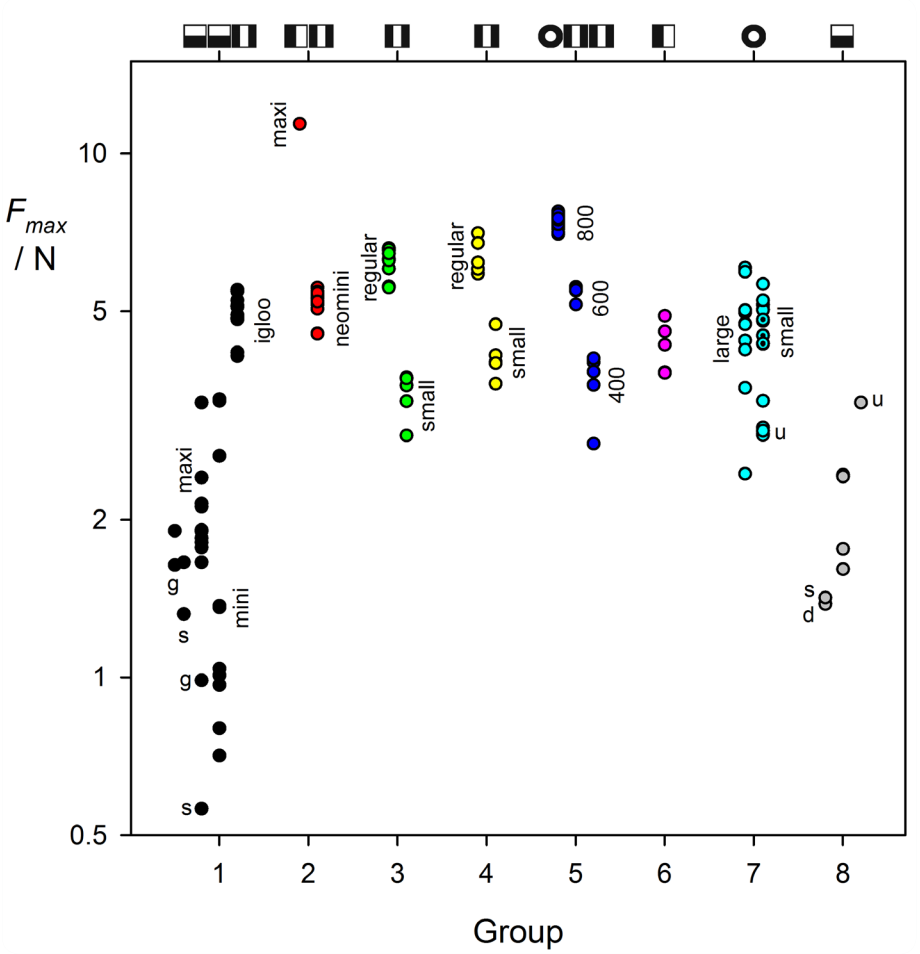

Figure 7: Breakaway force, F_{max}, by magnet type. Key as for Figure 4.

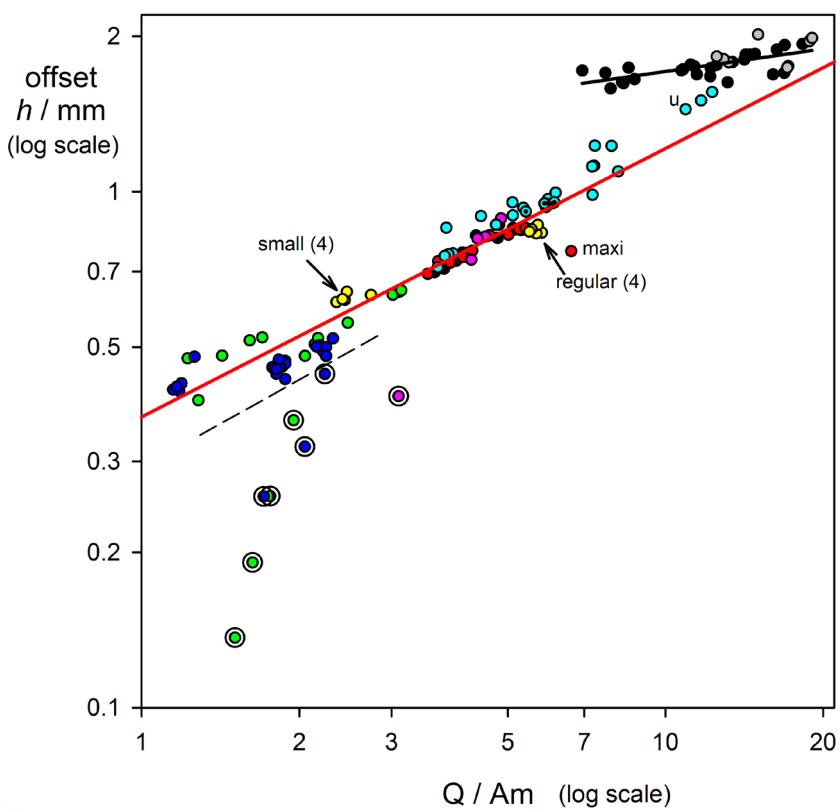

Figure 8: Offset *h* vs. Q. Separate regression lines shown for dipoles and the rest, the latter excluding those points below the dashed line, circled (see text). Group 2a and 4 magnets are labelled.

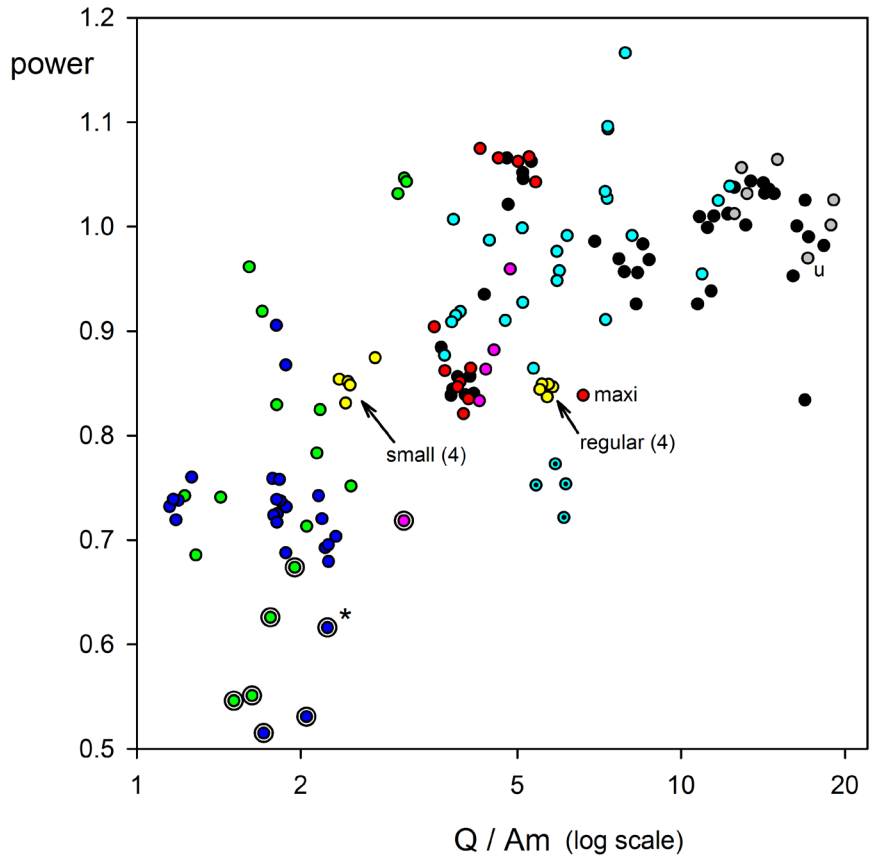

Figure 9: Stretch power, *c*, vs. Q. Group 2a and 4 magnets are labelled. Points excluded from regression Figure 8 circled, additionally identified aberrant instance with an asterisk.

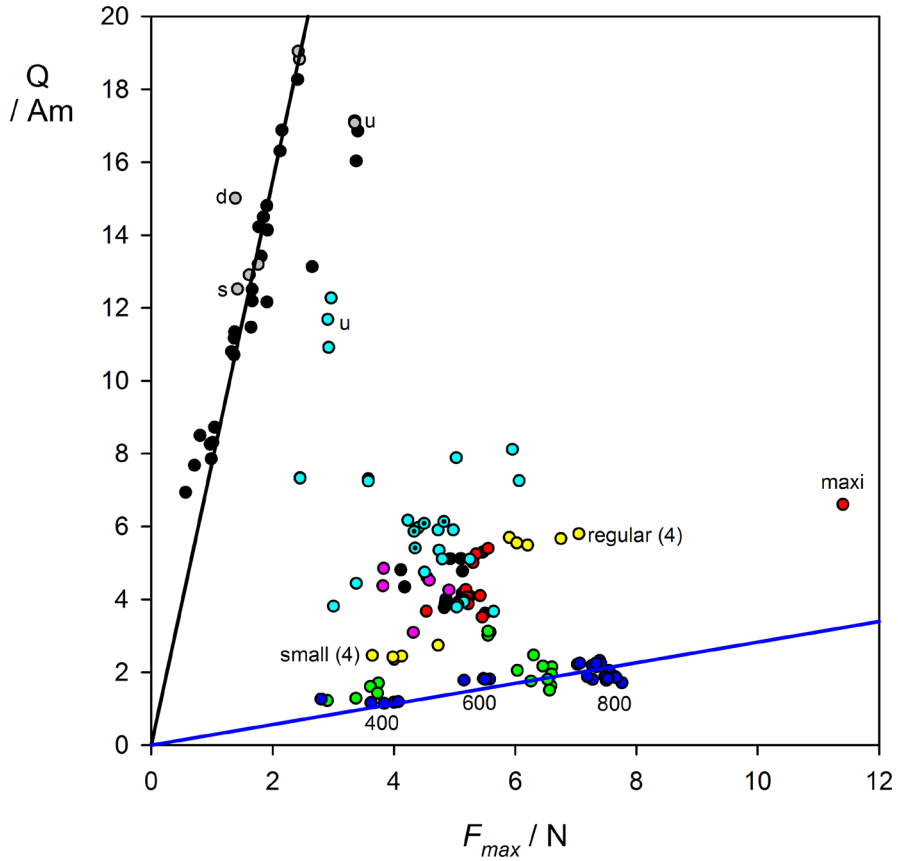

Figure 10: Q vs. F_{max}.Regression lines (constrained to the origin) for eye guidance for dipoles (excluding odd values to the right) and Group 5.

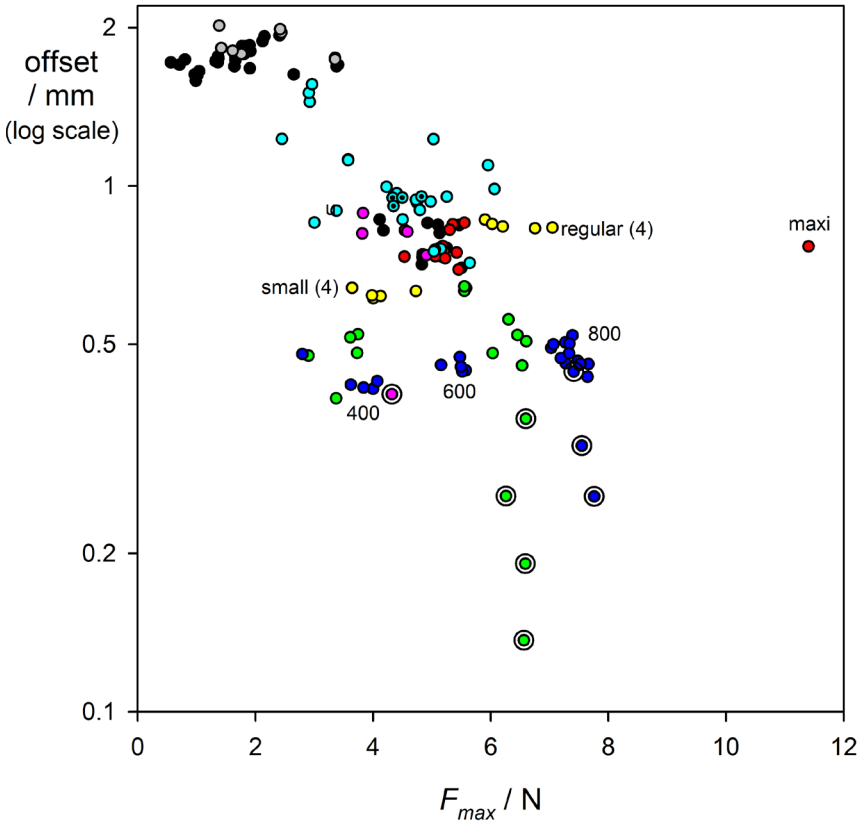

Figure 11: Offset *h* vs. F_{max}. Labelled as for Figure 9; Group 5 types also marked.

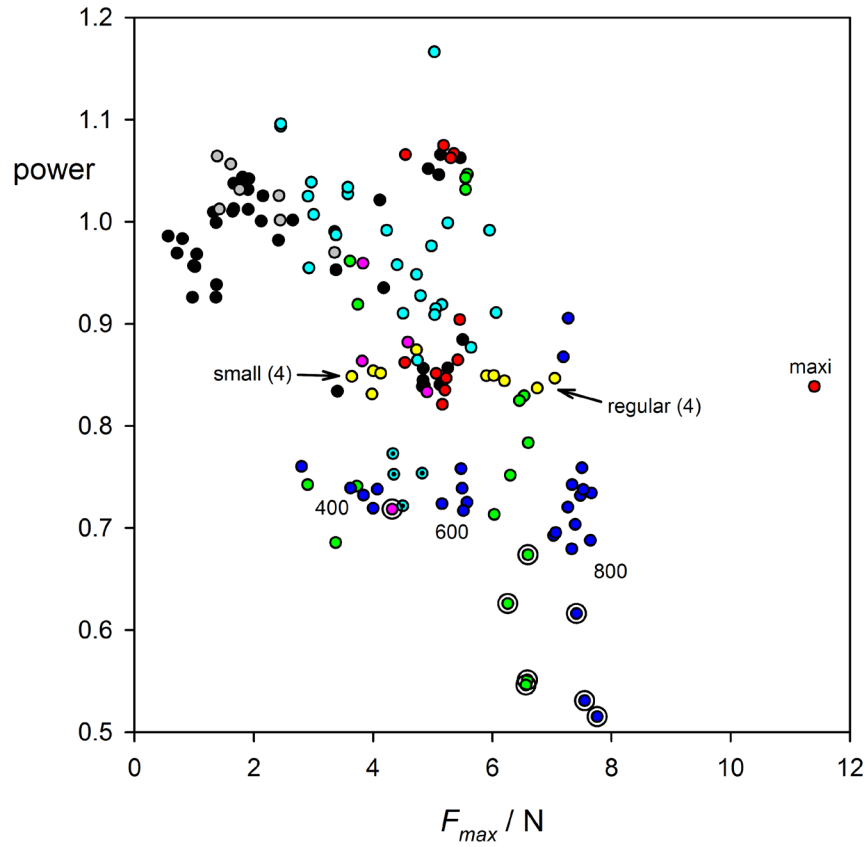

Figure 12: Stretch power, *c* vs. F_{max}. Labelled as for Figure 11.

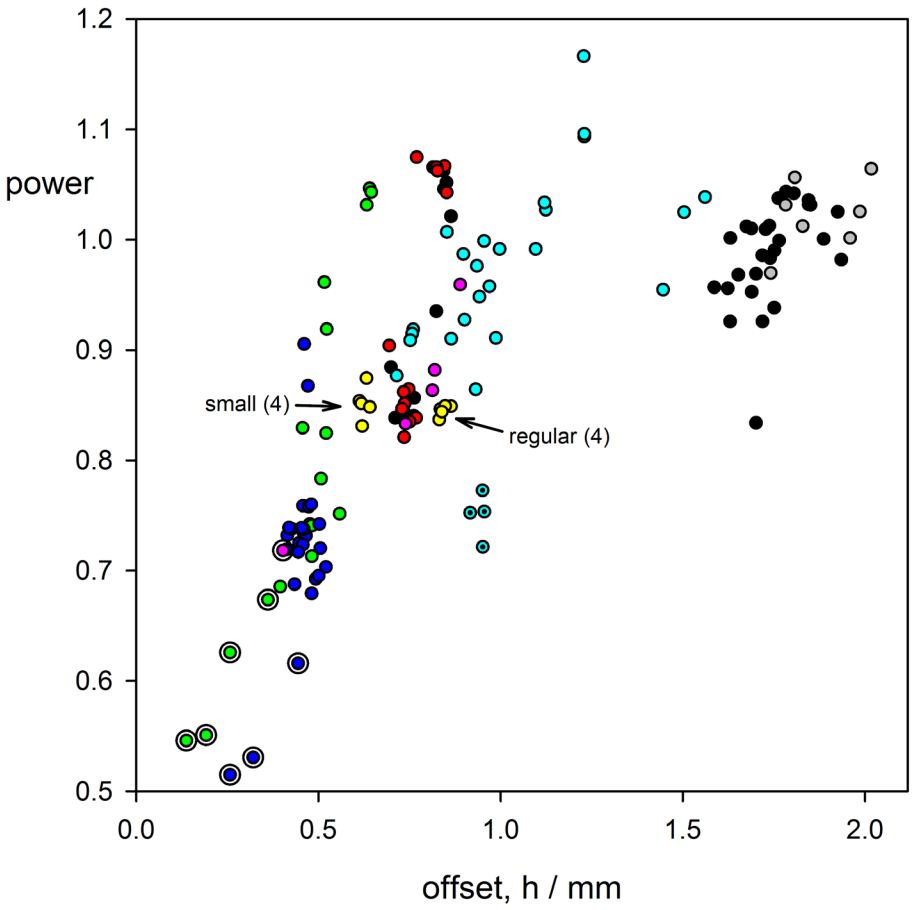

Figure 13: Stretch power, *c* vs. offset *h*. Labelled as for Figure 11.

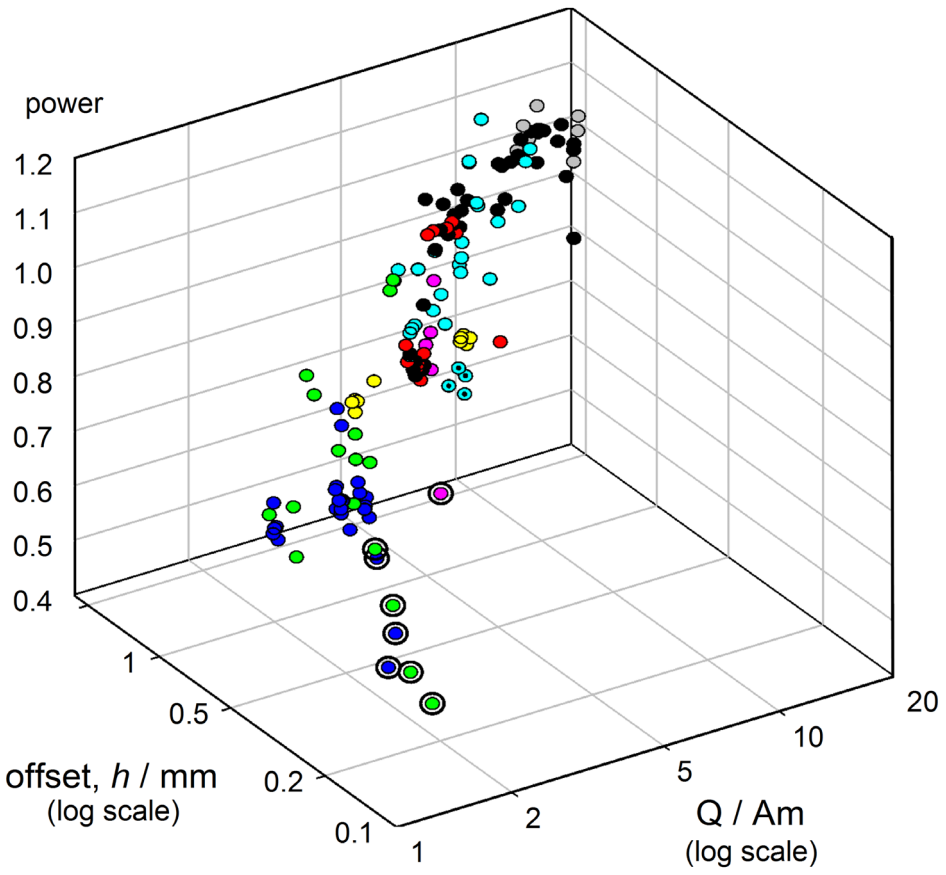

Figure 14: Stretch power, *c* vs. Q and offset, *h*.

now we have a much better idea of the behaviour of dental magnets than hitherto, in particular the limiting power law at large separations is now established unambiguously.

As noted above, the fitting process necessitated the use of error terms for force and distance in many instances. The distribution of these fitted error values for force is shown in Figure 15. Clearly this represents a mixed distribution in that the tails are unexpectedly long, given the central slope. However, while removing those tails leads to a closer approach to a normal distribution a proper dissection is not possible because it cannot be known what values in the central region belong to the broader distribution (which therefore cannot be analysed), but also these are censored data. That is, there are some 20 values missing because the fitted parameter was insignificant and dropped (due to spurious correlation between the fitted values). It is not possible now to identify the nature or source of the broader distribution, although the narrow distribution would appear to be on a reasonable scale to attribute it to simple random setting errors, although slightly biased (−0.0025 N ± 0.0032 N, manual estimate), at close to the resolution of the system. However, inspection of the error values by Group (*Supplementary Figure 1*) shows that the large errors were not randomly distributed but associated with particular instances in certain groups. The wholesale removal of data for individual magnet types from that error plot therefore was not appropriate as that kind of systematic effect was not in evidence.

The story for the distance error is rather different. These estimates were all positive, meaning that the fitted distance in these instances was always larger than that calculated as input (i.e. from the load cell relaxation correction), but distributed near normally as log values (*Figure 16*). Again,

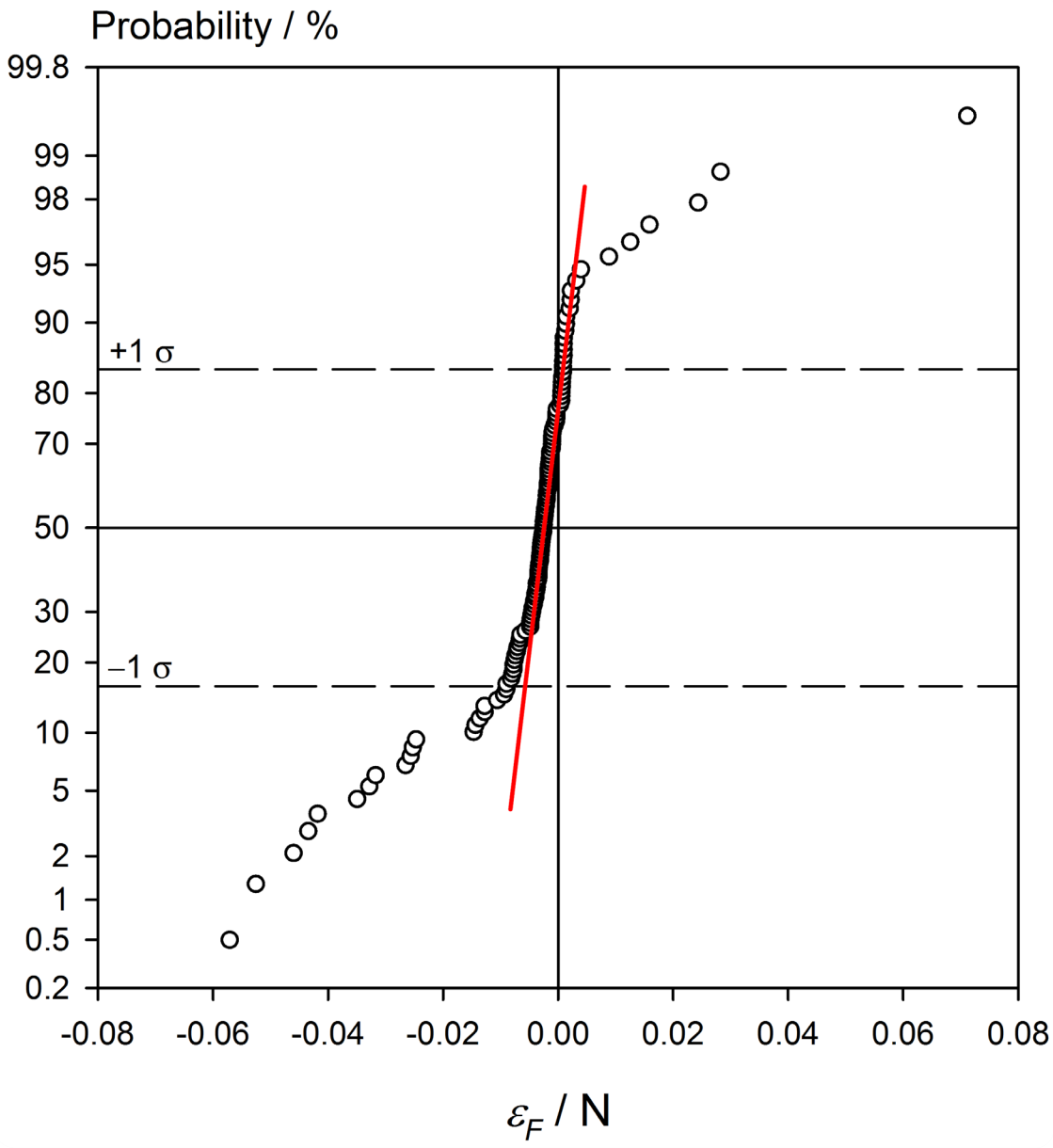

Figure 15: Distribution of fitted error values for force (Gaussian ordinate scale). Trend line of central region fitted by eye to show the disparity of the tails, implying a mixed distribution.

there is some censoring as the estimated values approach zero, non-significant values having to be dropped, that is there are missing values in the lower tail. The (geometric) mean would appear to be about 0.013 mm, and the effective standard deviation of the log of *d* about 0.608, or a factor of about 4 on *d* itself (from the regression, estimated s.d. = 1/slope, estimated mean = −intercept/slope). (These errors by Group are shown in Supplementary Figure 2.)

Inspection of the data for the runs where the *d* error term was required shows that it was restricted to products from Preat, Aichi and Technovent (Groups 3, 5 and 6) with the exception of a single instance for an Igloo magnet (Group 1c). From the details known *(Table 1)*, there is no evident commonality of design to distinguish this subset. While genuine experimental error would not be unreasonable and might have been expected (and indeed anticipated for the curve fitting), the brand coincidence suggests that another as yet unrecognized factor is operating, underlined by the fact that no negative values emerged, as would be expected for random setting errors.

The equation fitted (equation 1) was found by analogy with that for long thin dipoles,[2] merely changing the power law index from 2 to 4 after having excluded other possibilities. Strictly, the physically expected boundary condition at large separation of pure inverse 4th power is not satisfied, given that for many magnets a stretch power less than 1 is required for the fit. This might be attributed to real magnets having a behaviour differing from that assumed in,[5] specifically that the 'polar' patch is effectively movable, as previously discussed.[1,2] Indeed, the spatial distribution of the fictional magnetic poles may be responsive in some sense to the image interaction, as well as the location of the nominal polar disc relaxing, or being 'elastic', as previously suggested.[1] Nevertheless, the model does seem to be sufficient for general purposes *(Figure 3)*.

Turning to the principal fitted parameters, pole strength, Q, varied considerably between products *(Figure 4)*. Other than that the dipole magnets (1a, 1b, 8) had clearly higher values than the rest, and that physically larger magnets tended to show larger values, some more clearly than others, no clear pattern emerges. The use of commercial keepers (g, s, d) seem to show a tendency to slightly lower values, but given

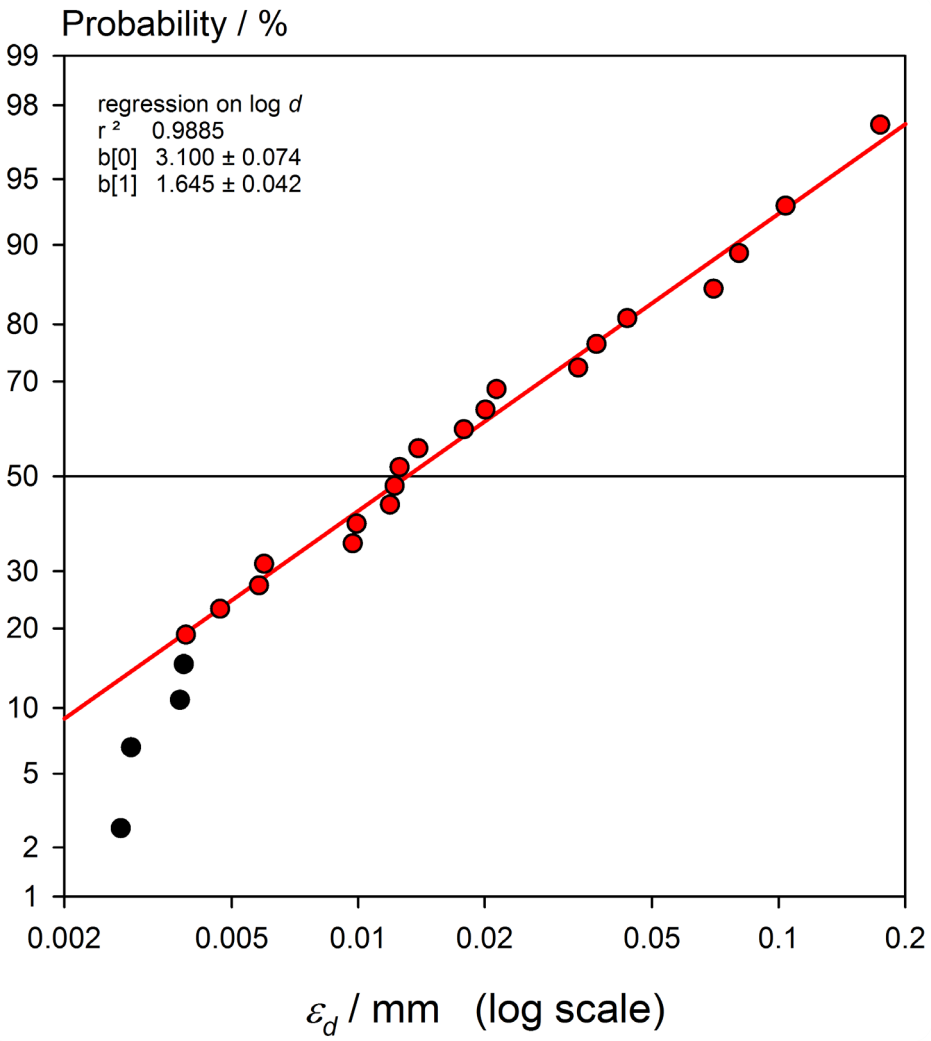

Figure 16: Distribution of fitted error values for distance (Gaussian ordinate scale). Trend line fitted after excluding lower four points (black).

the general scatter in replicates (*Supplementary Table 1*) this cannot be said with any certainty. In one instance (7b), removing the cladding resulted in an appreciable increase in Q, but not in the other that was attempted (8). This might be related to the assembly design, circular as opposed to dipole.

The distinction between the dipole types (1a, 1b, 8) and the others was much more marked in respect of the polar offset *(Figure 5*), the only exception being for the unclad 7b group. It is noted that this fitted value for the dipoles is a substantial fraction (~0.55 - 0.83) of the depth of the magnet (see Table 1), but for the others it ranged between ~0.04 and ~0.4. This underlines perhaps that the concept of a pole in such devices remains a 'convenient fiction',[1] but also that this is essentially from an arbitrary function fit. Even so, it does suggest a fundamental difference in behaviour when the polar axis is parallel as opposed to perpendicular to the permeable plane. It is necessary to note at this point that the working face of Group 4 magnets is spherically concave (the supplied keeper is correspondingly convex). This means that full contact was not obtained on the flat permeable plane. This does not appear to have affected the data fitting as such, but it suggests that the 'distance' is ambiguous and thus that the offset value is perhaps larger than otherwise would be the case; the effect however was not dramatic.

There is no clear pattern for the stretch power *(Figure 6*). Groups 1, 2b, 7 and 8 are centred on a value of ~1.0, Groups 1c, 4, and 6 are clustered in the vicinity of 0.85, while Groups 3 and 5 are centred on ~0.73. The others are not clear in this respect.

Where there is a clearer outcome is in respect of the breakaway force, F_{max} *(Figure 7*). The dipole types (1a, 1b, 8) gave much more widely scattered but generally appreciably lower values than the others which, somewhat surprisingly, show very little variation around a mean of about 5 N. However, while there is a clear size effect for Groups 2, 3, 4 and 5, this does not show for Group 7.

The variation of offset with Q is striking in a log-log plot *(Figure 8*). Firstly, the dipole magnets (1a, 1b, 8) fall clearly on a separate trajectory from the others, with a significant regression (solid black line): $r^2 = 0.4665$, n = 37, F = 30.6, P ~ 3×10^{-6}; $b_1 = 0.146 \pm 0.027$. The results for the other types also fall clearly on a line although there are a few points that have discrepant low values (circled, marked off by the dashed line). One of those points lies very close to that dashed line but was included because of the observation in respect of Figure 9 that lay in that subset there (see below). The regression on the remaining points (solid red line) is also highly significant: $r^2 = 0.9450$, n = 105, F = 17770, P ~ 1×10^{-66}; $b_1 = 0.561 \pm 0.013$. These results are taken to mean that there is some physical sense in the concept of offset, and dependent on Q, although of course quite what is not apparent. It may be noted that the difficulty with Group 4 noted above, with respect to the concavity, has not resulted in any great effect here.

The relationship of the fitted stretch power to pole strength, Q, is less clear *(Figure 9*). It is here, as before, an arbitrary means of adjusting the curvature, given that it is now understood that the near-field prediction of force is a complicated matter.[5] That said, it was noticed that 7 of the suspect points in Figure 8 were clustered together, but with a third member of Group 5a (asterisk) included in the region – hence the exclusion in Figure 8. On this view, then, there is still a trend from a low of about 0.7 to around 1.0, from low to high Q, but on this basis four data points for Group 7b seem to lie away from the others (dotted symbols). To examine whether this these points are associated with any other effects they are similarly identified in Figures 4 - 8, and 10 - 13, but nothing more obvious emerges.

If there is indeed a true relationship between these fitted parameters of offset and power on Q, the implication for the purpose of this curve-fitting exercise would be that they are essentially functions of Q and thus correlated with it. Ordinarily, such correlation causes problems in regression because it amounts to an overspecification, usually manifest by large significance probability values for the each of the variables so related. In each case here, however, after dropping the error terms on that basis, no non-significant inclusions were made in the final table of results. However, this does not eliminate co-dependence of the fitted parameters, meaning that it is feasible for odd values, such as now seen, to emerge in the course of the residuals minimization. Care is always required to avoid false imputations, hence the caution here.

The relationship of Q to the breakaway force, F_{max}, is more complicated *(Figure 10*). Firstly, with the exception of a few obvious outliers (see previous remarks), the dipole data (1a, 1b, 8) fall on a clear straight line through the origin (black) ($r^2 = 0.9914$, n = 23, F = 2536, P ~ 3×10^{-24}; $b_1 = 7.74 \pm 0.15$). Likewise, the data for Group 5 fall on a clear line through the origin (blue) ($r^2 = 0.9817$, n = 26, F = 1343, P ~ 3×10^{-23}; $b_1 = 0.283 \pm 0.008$). But while the data for Group 3 mostly fall fairly close to this latter line, the rest do not appear to have any systematic pattern, indeed they are very scattered. Thus while it might appear reasonable and expected for a direct relationship to exist, there are clearly other factors in play, including but probably not only experimental error.

While there is some clustering according to type, there is a general tendency to lower values of offset with increasing breakaway force *(Figure 11*) (a log scale for offset is used because it is considered infeasible for a negative value to arise at larger values of F_{max}). In the plot of power vs. breakaway force *(Figure 12*), there is a rather more obvious grouping into the sets mentioned for Figure 4, i.e. around 1.0, 0.85 and 0.73. With hindsight, this clustering can also be seen in Figure 9. If this effect is real it suggests that it may reflect the underlying physics, noticing that the dipoles and split-pole design (1a, 1b, 8) values lie around 1.0, the two split-pole designs have a value ~0.85, and that the values at ~0.73 are both sandwich types

– but the others confound this simplicity. Little of interest emerges in the plot of power vs. offset *(Figure 13*).

The 3-D view of power vs. offset and Q again shows that identifying the outlier points above was justified, but it does seem to point towards a structural relationship between these fitted parameters in what remains, of course, an approximating function.

Other possible relationships were explored — magnet dimensions, cross-section and volume, but most especially the fitted values against the actual contact area as this was postulated to be of some importance. However, apart from a vague general size effect, no new insight was gained.

In summary, the key finding now is that the predicted inverse fourth power for force vs. distance has been verified to apply to a variety of real dental magnets. Secondly, a usefully parsimonious function can be fitted to the data over a wide range, even if the form fails to meet the theoretical boundary condition. The calculated offset appears to be a direct function of effective pole strength, and of different form for dipoles as opposed to the other designs, which appear to have a common behaviour. Surprisingly, with the exception of dipoles (Groups 1, 8) and Groups 3 and 5, there is no clear relationship between apparent pole strength and the breakaway force *(Figure 10*).

Despite a great deal of attention being given to the form of the force-distance relationship for dental magnets, as documented before,[1,2] it remains unclear what practical benefit there is for dentistry as such, beyond the value of general understanding. It would appear that the only relevant property is the breakaway force, F_{max}, and this value in fact varies very little between the dental products examined here for all designs except simple open-field dipoles (low) and the example of a rather large Co-Sm device (Group 2a) (high) *(Figure 7*). There is therefore little to choose between them on that basis. Of course, this value is constrained by a minimum for a usefully functional retentive device, and a practical maximum for removal when required. Size may be more limiting in terms of prosthesis design.

CONCLUSION

The question of the power law applying to real dental magnets has been settled unambiguously, being inverse 4th power as predicted theoretically. However, the approximating function used now uses two parameters – offset and stretch power – that may suggest that the theoretically-assumed static magnetic pole distribution is in need of reconsideration, and thus whether they are functionally-related to pole strength or design. Clearly, the experimental difficulties discussed above need attention, if better resolution and reproducibility can be attained, for further study of the physics.

REFERENCES

1. Darvell, B.W. and Dias, A.P.L.H. Non-inverse-square force–distance law for long thin magnets. *Dent Mater* 2006; **22**:909-918.
2. Darvell, B.W. and Gilding, B.H. Non-inverse-square force–distance law for long thin magnets—Revisited. *Dent Mater* 2012; **28**:e42-e49.
3. Behrman, S.J. The implantation of magnets in the jaw to aid denture retention. *J Prosthet Dent* 1960; **10**:807-841.
4. Elliott, S.J. *The design of root caps for overlay dentures.* MDS dissertation. University of Sydney, 1988.
5. Darvell, B.W. and Gilding, B.H. The relationship between the force and separation of miniature magnets used in dentistry. *Dent Mater* 2018; **34**:e89-e106.
6. Dias, A.P.L.H. and Darvell, B.W. Physics, use and design of dental magnets. *J Jap Soc Mag Applic Dent* 1998; **7**:12-17.
7. Dias, A.P.L.H. *Aspects of the use and design of magnets in dentistry.* MPhil. The University of Hong Kong, 1999.
8. Tian, K. and Darvell, B.W. Determination of the flexural modulus of elasticity of orthodontic archwires. *Dent Mater* 2010; **26**:821-829.

SUPPLEMENTARY FIGURES AND TABLE

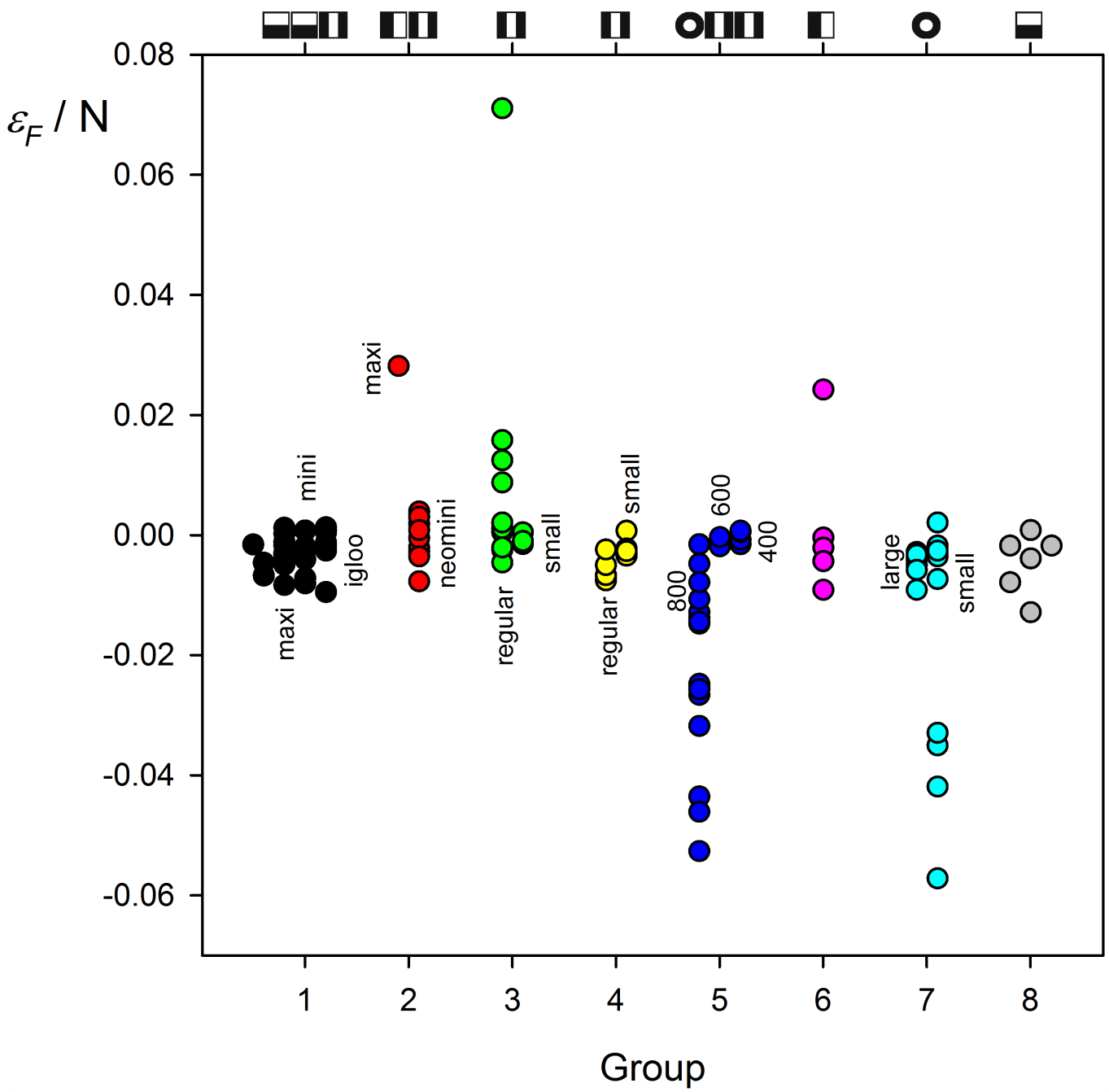

Supplementary Figure 1: Fitted values of zeroing error in *F*, ε_F

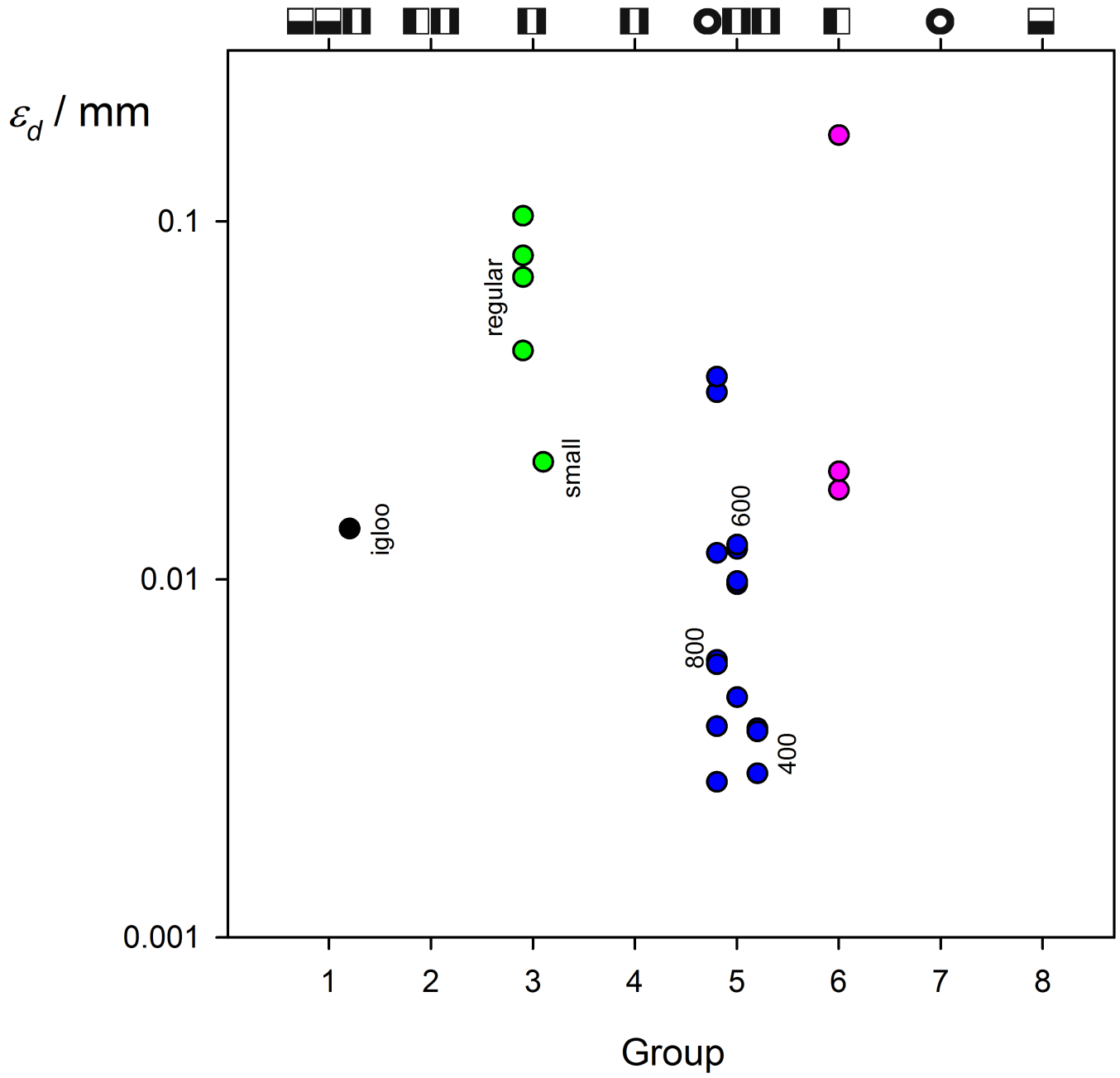

Supplementary Figure 2: Fitted values of zeroing error in *d*, ε_d.

Supplementary Table 1. Full fitted value data set.

				Fit parameters:	#A		#B		#D		#C		#E							
Company	Brand	Group	item no.	Notes	a	se(a)	h	se(h)	c	se(c)	eps_F	se(eps_F)	eps_d	se(eps_d)	r2	df adj r2	fit se	F-value	n	Q	Fmax
					strength		polar offset		stretch power		F error		d error								
GDP																					
	GDP Maxi	1a	1		21.016	0.338	1.844	0.011	1.036	7.31E-03	-2.91E-03	7.89E-04			0.999944	0.999935	4.06E-03	155676	30	14.497	1.845
			1		18.013	0.293	1.783	0.01	1.044	7.09E-03	-1.69E-03	6.28E-04			0.999944	0.999936	4.23E-03	161068.2	31	13.421	1.81
			1		20.247	0.348	1.845	0.011	1.032	7.47E-03	-4.22E-03	7.16E-04			0.999939	0.999929	4.38E-03	146567	31	14.229	1.77
			1		19.995	0.269	1.804	8.71E-03	1.042	5.89E-03	-3.79E-03	5.73E-04			0.999963	0.999956	3.47E-03	222412.2	29	14.14	1.912
			1		21.921	0.325	1.85	0.01	1.032	6.43E-03	-4.85E-03	6.62E-04			0.999955	0.999948	3.76E-03	198420.9	31	14.806	1.9
			2		15.655	0.249	1.761	0.01	1.038	7.04E-03	-3.22E-03	5.51E-04			0.999947	0.999938	4.17E-03	157212	29	12.512	1.66
			3		28.495	0.173	1.925	3.97E-03	1.025	1.07E-03	2.63E-04	1.10E-05			0.99999	0.99999	3.11E-03	5633989	176	16.881	2.15
			3		26.606	0.3	1.886	7.56E-03	1.001	4.83E-03	-8.24E-03	6.31E-04			0.999975	0.999971	2.77E-03	345491.3	30	16.311	2.12
			4		29.375	0.325	1.751	6.77E-03	0.99	2.80E-03	1.28E-03	1.44E-04			0.999917	0.999915	6.47E-03	576770.3	147	17.139	3.35
			5		33.373	0.084	1.934	1.65E-03	0.982	6.34E-04					0.999989	0.999989	1.24E-03	5173820	116	18.268	2.41
			1	GDP keeper	14.8	0.164	1.674	6.80E-03	1.012	4.78E-03	-1.53E-03	4.29E-04			0.999972	0.999968	3.00E-03	325235.5	31	12.166	1.905
			1	GDP keeper	13.168	0.136	1.687	6.21E-03	1.01	2.29E-03					0.999974	0.999971	2.80E-03	541049.9	31	11.475	1.64
			1	Shiner keeper	14.873	0.255	1.737	0.011	1.013	7.77E-03	-6.69E-03	7.48E-04			0.999939	0.999929	4.46E-03	131483.7	28	12.196	1.66
			1	Shiner keeper	11.668	0.169	1.727	8.65E-03	1.01	6.99E-03	-4.57E-03	6.56E-04			0.999956	0.999947	3.62E-03	166184.4	26	10.802	1.322
	GDP Mini	1b	1		17.248	1.26E-11	1.63	1.37E-12	1.002	1.18E-12	-4.01E-03	2.02E-15			0.99974	0.999714	0.0114	51299.16	44	13.133	2.65
			1		12.481	0.432	1.763	0.022	0.999	8.91E-03	-2.17E-03	2.10E-04			0.999821	0.999804	9.34E-03	78307.12	46	11.172	1.365
			1		11.483	0.072	1.718	3.82E-03	0.926	2.67E-03	8.25E-04	2.00E-04			0.999945	0.999944	3.59E-03	750654.8	127	10.716	1.361
			1		12.875	0.136	1.75	6.72E-03	0.938	4.64E-03	-8.00E-03	4.39E-04			0.999974	0.999969	2.77E-03	329080.8	30	11.347	1.37
			1		7.225	0.105	1.739	8.91E-03	0.984	3.56E-03					0.999945	0.999937	3.65E-03	216611.5	27	8.5	0.8
			1		5.894	0.077	1.7	7.95E-03	0.969	3.70E-03					0.999948	0.99994	3.23E-03	193936.7	23	7.677	0.71
			1		6.914	0.106	1.623	8.95E-03	0.956	3.65E-03					0.999939	0.999931	4.03E-03	196047.2	27	8.315	1.01
			1		7.616	0.14	1.652	0.011	0.968	7.92E-03	-1.86E-03	4.31E-04			0.999919	0.999906	5.04E-03	111013.7	31	8.727	1.04
			1		6.827	0.094	1.629	7.38E-03	0.926	6.39E-03	-7.13E-03	5.69E-04			0.999959	0.999951	3.26E-03	172623.2	25	8.263	0.968
			2		28.423	0.198	1.7	2.77E-03	0.834	2.11E-03					0.99997	0.999967	6.95E-04	607517.5	40	16.859	3.4
			2		25.718	0.281	1.688	6.58E-03	0.953	3.45E-03	-2.49E-03	3.22E-04			0.999887	0.999884	6.58E-03	393717.4	137	16.037	3.375
			1	GDP keeper	6.174	0.094	1.585	8.67E-03	0.957	3.38E-03					0.999946	0.99994	4.09E-03	233341.3	28	7.857	0.988
			1	Shiner keeper	4.812	0.087	1.717	0.011	0.986	7.83E-03	-1.10E-03	2.39E-04			0.999925	0.999914	4.81E-03	120211	31	6.937	0.562
	Igloo	1c	1		2.31	0.031	0.863	5.26E-03	1.021	5.83E-03	-1.20E-03	2.80E-04			0.999943	0.999933	5.59E-03	129371.6	26	4.806	4.11
			1		1.446	0.013	0.733	2.42E-03	0.845	3.45E-03	6.25E-04	1.70E-04			0.99994	0.999936	7.78E-03	353596.7	68	3.803	4.835
			2		1.424	0.034	0.709	0.015	0.839	5.79E-03	1.35E-03	1.53E-04	0.014	6.69E-03	0.999976	0.999975	4.84E-03	669349.9	68	3.774	4.828
			2		2.613	0.035	0.85	5.27E-03	1.052	3.17E-03					0.999941	0.999934	5.86E-03	220652.8	29	5.111	4.925
			3		1.672	0.012	0.762	1.97E-03	0.857	2.67E-03	8.95E-04	1.20E-04			0.999965	0.999963	6.00E-03	627954.9	69	4.089	5.25
			3		1.886	0.031	0.823	6.48E-03	0.935	6.49E-03	-1.67E-03	2.59E-04			0.999903	0.999889	7.65E-03	93155.71	31	4.343	4.175
			3		1.311	0.017	0.698	4.30E-03	0.885	5.90E-03	-9.46E-03	4.64E-04			0.999935	0.999921	6.25E-03	97833.51	23	3.62	5.5
			3		1.604	0.01	0.74	2.15E-03	0.839	1.19E-03					0.999941	0.999939	5.61E-03	1080613	131	4.005	4.858
			3		1.725	0.015	0.761	3.26E-03	0.84	3.33E-03	-2.55E-03	2.02E-04			0.999967	0.999962	4.20E-03	264141.5	30	4.154	5.12
			3		2.806	0.049	0.843	6.77E-03	1.063	4.06E-03					0.999903	0.999891	7.59E-03	133456.4	29	5.298	5.46
			4		1.505	0.012	0.741	2.22E-03	0.857	2.98E-03	9.44E-04	1.19E-04			0.999953	0.99995	7.14E-03	474888.1	71	3.88	4.838
			4		2.283	0.046	0.814	7.64E-03	1.066	7.21E-03	5.01E-04	1.89E-04			0.99989	0.999872	8.68E-03	78492.03	30	4.779	5.128
			5		2.62	0.038	0.843	5.54E-03	1.046	3.33E-03					0.999933	0.999925	6.21E-03	195032.8	29	5.118	5.1
Innovadent																					
	Maxi	2a	1		4.364	0.05	0.767	3.54E-03	0.839	5.73E-03	0.028	1.89E-03			0.999664	0.999651	9.16E-03	109023.6	114	6.606	11.4
	Neomini	2b	1		1.651	0.015	0.749	3.42E-03	0.835	3.69E-03	-7.64E-03	2.50E-04			0.999966	0.99996	4.50E-03	226817.9	27	4.063	5.2
			2		2.753	0.057	0.845	7.98E-03	1.067	5.37E-03					0.999858	0.999837	8.71E-03	77186.55	25	5.247	5.35
			2		1.581	8.04E-03	0.734	1.98E-03	0.821	2.47E-03	1.95E-03	1.88E-04			0.999934	0.999932	4.65E-03	589667.7	121	3.976	5.16
			2		1.537	0.012	0.735	2.25E-03	0.852	1.99E-03					0.999946	0.999943	7.31E-03	587843.3	67	3.921	5.057
			2		1.236	0.028	0.694	7.95E-03	0.904	8.93E-03	-3.48E-03	3.58E-04			0.999796	0.999762	0.0117	40897.48	29	3.515	5.45
			3		2.914	0.016	0.851	2.18E-03	1.043	2.79E-03	-2.65E-03	1.83E-04			0.999989	0.999986	2.28E-03	505083.9	21	5.398	5.55
			3		1.682	0.013	0.747	2.23E-03	0.865	2.53E-03	3.96E-03	6.53E-05			0.999964	0.999962	6.59E-03	732066.6	83	4.101	5.419
			4		2.125	0.048	0.823	8.08E-03	1.066	0.012	-2.04E-03	8.24E-04			0.999844	0.999805	9.09E-03	36371.87	21	4.61	4.54
			4		1.5042	0.012	0.728	2.20E-03	0.847	2.98E-03	3.08E-03	1.27E-04			0.999955	0.999952	6.87E-03	489162.9	70	3.878	5.221
			5		1.823	0.031	0.769	6.21E-03	1.075	5.69E-03					0.999881	0.999857	7.54E-03	67295.23	19	4.27	5.18
			5		1.353	0.011	0.734	2.24E-03	0.862	2.49E-03	8.75E-04	4.60E-05			0.999959	0.999957	7.45E-03	638506.8	82	3.678	4.53
			6		2.5104	0.042	0.826	6.48E-03	1.063	6.17E-03	-4.43E-04	1.85E-04			0.99992	0.999907	7.24E-03	107981.5	30	5.01	5.3
Preat																					
	Shiner Re	3a	1		0.458	0.01	0.507	2.93E-03	0.784	6.02E-03	0.016	1.81E-03			0.999771	0.999761	6.39E-03	128229.8	92	2.139	6.6
			1		0.959	0.022	0.64	7.64E-03	1.047	0.01	6.69E-04	2.26E-04			0.999787	0.999748	0.012	35916.2	27	3.097	5.58
			1	x	0.379	0.029	0.361	0.033	0.674	0.013	5.33E-04	2.45E-04	0.044	0.011	0.999938	0.999933	8.06E-03	251590.2	67	1.948	6.596
			1	x	0.309	0.017	0.257	0.022	0.626	9.21E-03	-2.41E-03	2.19E-04	0.08	7.39E-03	0.999944	0.999942	5.27E-03	912402.5	211	1.758	6.255
			2		0.909	0.021	0.631	7.57E-03	1.032	8.61E-03	1.19E-03	1.46E-04			0.999798	0.999764	0.0121	41188.46	29	3.014	5.55
			3		0.978	0.023	0.644	7.89E-03	1.043	0.011	2.14E-03	3.02E-04			0.999757	0.999711	0.0123	30200.59	26	3.127	5.55
			3		0.42	0.013	0.481	6.25E-03	0.713	0.01	8.82E-03	4.31E-04			0.999155	0.999107	0.0297	27984.66	75	2.049	6.03
			3	x	0.265	0.032	0.191	0.047	0.551	0.024	0.013	2.43E-03	0.07	0.011	0.999991	0.999991	1.53E-03	2914368	105	1.627	6.585
			3		0.326	9.16E-03	0.456	2.55E-03	0.83	6.11E-03	0.071	2.30E-03			0.999791	0.999786	7.96E-03	284107.7	162	1.806	6.531
			3	x	0.227	0.014	0.137	0.021	0.546	9.16E-03	-4.53E-03	3.94E-04	0.104	5.92E-03	0.999984	0.999984	2.35E-03	3011534	197	1.506	6.562
			3		0.47	7.45E-03	0.521	4.79E-03	0.825	6.00E-03	-2.01E-03	1.58E-04			0.999861	0.999838	0.0102	59910.99	29	2.169	6.45
			4		0.611	4.46E-03	0.557	2.30E-03	0.752	1.62E-03					0.999964	0.99996	4.40E-03	363242.9	29	2.471	6.3
	Shiner Sm	3b	1		0.288	6.04E-03	0.522	6.25E-03	0.919	5.23E-03					0.999747	0.999716	0.0131	49465.35	28	1.698	3.74
			2		0.258	4.61E-03	0.515	5.16E-03	0.962	7.74E-03	4.88E-04	9.62E-05			0.999833	0.999803	0.011	45969.54	27	1.607	3.61
			3		0.164	4.11E-03	0.395	0.012	0.686	6.02E-03	-1.43E-03	8.47E-05	0.021	3.46E-03	0.999945	0.999942	4.62E-03	507311.3	117	1.282	3.37
			3		0.15	4.04E-03	0.476	6.09E-03	0.742	0.01	-1.13E-03	2.64E-04			0.999681	0.999611	0.0142	19871.57	23	1.223	2.9
			3		0.203	2.28E-03	0.481	3.05E-03	0.741	4.27E-03	-9.41E-04	9.55E-05			0.999922	0.999908	7.14E-03	102077.2	28	1.424	3.725
SSI																					
	Jackson Re	4a	1		3.365	0.053	0.834	6.20E-03	0.847	5.91E-03	-6.82E-03	5.37E-04			0.999906	0.9999	6.96E-03	92630.46	30	5.801	7.05
			2		3.21	0.039	0.831	4.73E-03	0.837	4.87E-03	-7.48E-03	5.79E-04			0.999941	0.99993	5.35E-03	135054.8	28	5.666	6.75
			3		3.246	0.039	0.863	4.77E-03	0.849	4.63E-03	-6.62E-03	4.26E-04			0.999951	0.999942	5.11E-03	161813.3	28	5.698	5.9
			4		3.074	0.046	0.847	6.01E-03	0.849	5.61E-03	-4.94E-03	4.73E-04			0.999914	0.9999	6.65E-03	104087.3	31	5.544	6.02
			5		3.014	0.053	0.838	6.89E-03	0.844	6.57E-03	-2.36E-03	5.85E-04			0.999878	0.999859	7.72E-03	73701.97	31	5.49	6.2

Supplementary Table 1 continued overleaf...

Supplementary Table 1 continued...

	Jackson Sr	4b	1		0.75	0.01	0.631	4.32E-03	0.875	5.45E-03	-3.40E-03	2.00E-04			0.999923	0.9999	7.23E-03	99743.01	27	2.738	4.725
			2		0.553	8.13E-03	0.612	4.75E-03	0.854	3.84E-03					0.99988	0.999864	8.22E-03	95960.44	26	2.353	4
			3		0.596	6.44E-03	0.617	3.26E-03	0.852	4.57E-03	7.87E-04	1.93E-04			0.999946	0.999936	5.54E-03	135364.4	26	2.44	4.125
			4		0.606	7.50E-03	0.64	3.89E-03	0.849	5.82E-03	-2.20E-03	2.10E-04			0.999937	0.999922	6.35E-03	95470.98	22	2.462	3.64
			5		0.583	6.74E-03	0.619	3.25E-03	0.831	4.84E-03	-2.62E-03	2.64E-04			0.999948	0.999936	5.46E-03	121002.6	23	2.415	3.98
Aichi																					
	Magfit Ma	5a	1		0.537	7.37E-03	0.52	1.91E-03	0.703	3.92E-03	-0.027	1.22E-03			0.999894	0.999888	4.89E-03	219826.9	74	2.317	7.39
			1	x	0.5	4.38E-03	0.444	7.38E-03	0.616	7.34E-03	-0.043	1.55E-03	0.012	1.35E-03	0.999987	0.999986	1.62E-03	1265823	71	2.237	7.412
			1		0.325	8.37E-03	0.46	6.46E-03	0.906	0.014	-1.46E-03	1.81E-04			0.999833	0.999722	0.0155	13968.68	11	1.802	7.274
			1		0.352	2.94E-03	0.47	2.02E-03	0.868	6.66E-03	-4.72E-03	2.46E-04			0.999958	0.999947	4.73E-03	127109.6	20	1.877	7.192
			1		0.478	4.04E-03	0.504	9.77E-04	0.72	1.62E-03	-0.032	8.32E-04			0.999985	0.999984	1.62E-03	1213169	58	2.186	7.269
			1		0.491	2.40E-03	0.492	2.74E-03	0.693	4.01E-03	-0.025	7.69E-04	3.89E-03	6.38E-04	0.999992	0.999991	1.38E-03	1822189	62	2.216	7.023
			1		0.505	3.00E-03	0.5	2.87E-03	0.696	4.59E-03	-0.025	9.11E-04	2.72E-03	6.46E-04	0.999989	0.999988	1.62E-03	1288474	62	2.247	7.062
			2	x	0.419	0.013	0.32	0.016	0.531	0.011	-0.053	2.12E-03	0.033	2.50E-03	0.999988	0.999987	1.53E-03	1385783	71	2.047	7.548
			2		0.464	3.42E-03	0.502	1.41E-03	0.742	3.00E-03	-0.014	4.24E-04			0.999934	0.99993	4.64E-03	376847.2	79	2.154	7.338
			2		0.505	2.61E-03	0.481	4.16E-03	0.679	5.05E-03	-0.026	9.10E-04	5.96E-03	9.36E-04	0.999988	0.999987	1.70E-03	1389232	74	2.248	7.333
			3	x	0.292	0.03	0.257	0.045	0.515	0.027	-0.046	3.65E-03	0.037	6.93E-03	0.999906	0.999899	4.76E-03	180250.9	73	1.708	7.759
			3		0.352	5.83E-03	0.434	0.011	0.688	0.011	-0.013	9.79E-04	5.79E-03	2.39E-03	0.999895	0.999888	5.67E-03	173530.9	78	1.877	7.646
			3		0.343	2.87E-03	0.458	1.63E-03	0.734	3.32E-03	-0.011	3.99E-04			0.999906	0.999901	5.61E-03	266326.7	79	1.853	7.662
			4		0.353	1.53E-03	0.465	5.96E-04	0.732	1.37E-03	-0.015	2.91E-04			0.999986	0.999986	1.89E-03	1746775	75	1.879	7.479
			4		0.315	2.40E-03	0.457	1.77E-03	0.759	3.40E-03	-7.79E-03	2.46E-04			0.999903	0.999898	6.39E-03	269348.2	82	1.775	7.503
			4		0.336	1.35E-03	0.459	6.65E-04	0.738	1.47E-03	-0.014	2.20E-04			0.999983	0.999982	2.28E-03	1432743	77	1.833	7.525
	Magfit EX	5b	1		0.333	0.01	0.473	0.013	0.758	8.04E-03	-3.83E-04	1.26E-04	4.69E-03	4.14E-03	0.999895	0.999886	0.0114	147388.8	67	1.826	5.474
			2		0.327	0.013	0.446	0.019	0.725	0.011	-1.10E-03	3.32E-04	0.0122	5.79E-03	0.999904	0.999895	9.24E-03	138502.4	58	1.809	5.573
			3		0.318	0.011	0.457	0.016	0.724	0.01	-1.06E-03	2.48E-04	9.69E-03	4.72E-03	0.999912	0.999903	9.28E-03	155640.3	60	1.782	5.154
			4		0.326	0.013	0.444	0.019	0.717	0.012	-1.84E-03	3.73E-04	0.0125	5.69E-03	0.999903	0.999894	9.12E-03	134376.8	57	1.807	5.513
			5		0.326	0.014	0.453	0.02	0.739	0.012	-2.79E-04	2.83E-04	9.89E-03	6.14E-03	0.999864	0.999852	0.0117	103234.6	61	1.806	5.49
	Magfit EX	5c	1		0.159	1.12E-03	0.479	1.54E-03	0.76	2.18E-03					0.999929	0.9999	7.94E-03	371883.5	56	1.26	2.795
			2		0.139	2.34E-03	0.411	7.80E-03	0.719	8.16E-03	-1.49E-03	2.44E-04	3.84E-03	2.07E-03	0.999926	0.999917	7.59E-03	157774.5	52	1.178	3.998
			3		0.132	2.44E-03	0.414	8.07E-03	0.732	7.79E-03	-7.11E-04	1.55E-04	2.88E-03	2.18E-03	0.99991	0.999901	9.37E-03	138544	55	1.148	3.835
			4		0.142	1.63E-03	0.425	1.82E-03	0.738	4.02E-03	5.51E-04	1.42E-04			0.999925	0.999919	7.93E-03	227232.9	55	1.191	4.067
			5		0.136	3.06E-03	0.419	0.01	0.739	8.73E-03	7.62E-04	1.53E-04	3.76E-03	2.89E-03	0.999898	0.999888	0.0101	130090.8	58	1.166	3.619
Technovent																					
	Magna-ca	6	1		2.045	0.015	0.818	2.31E-03	0.882	4.09E-03	0.024	1.29E-04			0.999979	0.999974	2.27E-03	316173.2	34	4.522	4.578
			2		2.351	0.077	0.888	0.013	0.96	7.63E-03	-3.68E-04	5.10E-05			0.999754	0.999714	0.0131	33933.31	29	4.849	3.827
			2		1.91	0.041	0.812	0.016	0.864	4.85E-03	-2.05E-03	1.30E-04	0.0178	7.99E-03	0.999975	0.999973	4.05E-03	917925.9	98	4.371	3.815
			3		1.81	0.042	0.738	0.016	0.834	5.63E-03	-4.31E-03	2.28E-04	0.02	7.08E-03	0.999968	0.999966	4.35E-03	689699.5	94	4.254	4.903
			4	x	0.956	0.198	0.402	0.109	0.718	0.031	-9.04E-04	9.87E-04	0.1741	0.05	0.999923	0.999919	5.88E-03	274266.7	89	3.091	4.318
Magne-dent																					
	MagneDe	7a	1		3.559	0.167	0.968	0.02	0.958	0.02	-3.59E-03	1.29E-03			0.999317	0.9992	0.0189	12192.78	29	5.9655	4.4
			1		2.859	0.06	0.931	9.06E-03	0.865	0.011	-4.93E-03	1.17E-03			0.998977	0.998939	0.0159	35804.96	114	5.347	4.74
			2		3.489	0.138	0.941	0.017	0.948	0.017	-3.80E-03	1.15E-03			0.999517	0.999433	0.0162	16559.2	28	5.907	4.725
			3		3.487	0.138	0.934	0.016	0.976	9.20E-03					0.999485	0.999425	0.0163	26176.72	30	5.905	4.975
			4		6.221	0.271	1.227	0.023	1.166	0.014	-2.77E-03	3.04E-04			0.999937	0.999927	6.59E-03	137515.9	24	7.887	5.025
			4		5.34	0.209	1.123	0.018	1.027	0.016	-4.02E-03	9.18E-04			0.999671	0.999611	0.0139	23275.85	27	7.308	3.575
			4		5.378	0.114	1.228	0.01	1.094	9.07E-03	-3.34E-03	3.89E-04			0.999894	0.999876	7.38E-03	75532.51	28	7.333	2.45
			4		5.249	0.208	1.119	0.018	1.034	0.016	-3.08E-03	7.99E-04			0.999615	0.999556	0.0145	23356.57	31	7.245	3.575
			4		5.371	0.119	1.228	0.011	1.096	9.36E-03	-3.11E-03	3.81E-04			0.999888	0.999869	7.69E-03	74467.47	29	7.329	2.45
			4		5.266	0.263	0.986	0.022	0.911	0.019	-9.05E-03	1.63E-03			0.999256	0.999141	0.0198	12086.35	31	7.257	6.06
			4		6.597	0.158	1.095	0.011	0.992	8.57E-03	-3.22E-03	4.18E-04			0.999316	0.999293	0.0184	60350.95	128	8.122	5.95
			5		3.805	0.172	0.996	0.02	0.992	0.017	-5.73E-03	7.89E-04			0.999473	0.999392	0.018	17058.73	31	6.168	4.225
	MagneDe	7b	1		1.54	0.083	0.759	0.02	0.919	0.02	-1.89E-03	7.65E-04			0.998933	0.998768	0.026	8423.017	31	3.925	5.15
			1		1.348	0.071	0.714	0.019	0.877	0.02	-3.44E-03	8.79E-04			0.998963	0.998774	0.0264	7383.922	27	3.672	5.64
			1		1.453	0.056	0.852	0.015	1.007	9.14E-03					0.999497	0.999442	0.0176	27840.23	31	3.812	3
			1		1.481	0.081	0.756	0.02	0.915	0.021	-2.83E-03	7.27E-04			0.998909	0.998741	0.0267	8241.365	31	3.848	5.05
			1		1.432	0.083	0.751	0.022	0.909	0.022	-2.32E-03	7.96E-04			0.998754	0.998555	0.0284	6949.071	30	3.785	5.03
			2		1.971	0.102	0.897	0.021	0.987	0.021	-3.04E-03	7.78E-04			0.999175	0.999032	0.0223	9693.395	28	4.44	3.375
			2		1.97	0.1	0.897	0.021	0.987	0.021	-3.00E-03	7.49E-04			0.99922	0.99909	0.0219	10673.52	29	4.439	3.375
			2		2.252	0.119	0.863	0.021	0.91	0.02	-3.48E-03	9.50E-04			0.999059	0.998914	0.0233	9553.266	31	4.746	4.5
			3		2.6	0.076	0.954	0.015	0.999	0.017	-7.25E-03	1.12E-03			0.999918	0.999896	5.56E-03	64773.35	21	5.099	5.25
			3		2.609	0.089	0.9	0.011	0.928	0.013	-1.72E-03	4.70E-04			0.999332	0.999291	0.0261	32912.3	70	5.108	4.794
			4	e	3.442	0.118	0.949	8.00E-03	0.773	0.011	-0.035	3.28E-03			0.999616	0.999583	0.0126	41663.38	52	5.867	4.331
			4	e	3.703	0.143	0.95	8.33E-03	0.722	0.01	-0.057	4.72E-03			0.999692	0.999664	0.01	48707.76	49	6.085	4.496
			4	e	3.764	0.139	0.954	8.45E-03	0.754	0.012	-0.042	4.21E-03			0.999615	0.999581	0.012	39820.82	50	6.135	4.822
			5	e	2.923	0.103	0.915	8.08E-03	0.753	0.012	-0.033	3.22E-03			0.999573	0.999537	0.0134	37495.48	52	5.406	4.345
			1	unclad	11.922	0.128	1.445	5.65E-03	0.955	2.27E-03					0.999833	0.999829	7.31E-03	380455	130	10.919	2.92
			1	unclad	13.658	0.476	1.503	0.019	1.025	8.75E-03	-2.54E-03	2.41E-04			0.999818	0.999801	0.0105	77068.4	46	11.687	2.905
			1	unclad	15.066	0.12	1.561	4.62E-03	1.039	2.03E-03	2.13E-03	5.11E-05			0.999976	0.999975	3.74E-03	1919766	133	12.274	2.96
Dyna Dental																					
	Dyna	8	1		17.42	0.252	1.781	9.33E-03	1.032	6.40E-03	-3.85E-03	5.60E-04			0.999955	0.999948	3.78E-03	193346.5	30	13.198	1.76
			1		16.663	0.424	1.807	0.016	1.057	5.83E-03					0.999863	0.999846	6.46E-03	94691.81	29	12.909	1.61
			2		35.45	0.527	1.958	0.01	1.002	6.41E-03	-0.013	1.02E-03			0.999958	0.999951	3.56E-03	204225.7	30	18.828	2.44
			2		36.279	0.226	1.985	4.23E-03	1.026	1.80E-03	8.90E-04	1.12E-04			0.999978	0.999977	3.00E-03	2047060	138	19.047	2.42
			2	Dyna keeper	22.539	0.309	2.016	0.01	1.064	6.16E-03	-1.70E-03	5.12E-04			0.999965	0.999959	3.22E-03	245412.3	30	15.013	1.382
			2	Shiner keeper	15.674	0.238	1.828	0.01	1.013	7.50E-03	-7.81E-03	8.22E-04			0.999949	0.99994	3.74E-03	150891.3	27	12.52	1.42
			1	unclad	29.154	0.276	1.74	5.90E-03	0.97	3.42E-03	-1.70E-03	4.10E-04			0.999902	0.999899	5.51E-03	439688.7	133	17.074	3.35
				x : see Fig 8																	
				e : see Fig 9																	